Microengineered $CH_3NH_3PbI_3$ Nanowire/Graphene Phototransistor for Low-Intensity Light Detection at Room Temperature

*Massimo Spina, Mario Lehmann, Bálint Náfrádi, Laurent Bernard, Eric Bonvin, Richard Gaál, Arnaud Magrez, László Forró, and Endre Horváth**

Methylammonium lead iodide perovskite has revolutionized the field of third-generation solid-state solar cells leading to simple solar cell structures.[1] and certified efficiencies up to 20.1%.[2] Recently the peculiar light-harvesting properties of organometal halide perovskites have been exploited in photodetectors where responsivities of ≈3.5 A W^{-1} and 180 A W^{-1} have been, respectively, achieved for pure perovskite-based devices[3] and hybrid nanostructures.[4] Here, we report on the first hybrid phototransistors where the performance of a network of photoactive methylammonium lead iodide nanowires (hereafter $MAPbI_3NW$) is enhanced by chemical vapour deposition (CVD) grown monolayer graphene. These devices show responsivities as high as ≈2.6×10^6 A W^{-1} in the visible range showing potential as room-temperature single-electron detectors.

Certain characteristics (i.e., direct bandgap,[5] large absorption coefficient,[6] long charge diffusion lengths.[7] make $MAPbI_3$ appealing for several optoelectronic applications. In optoelectronic devices, it was first introduced as a sensitizer in dye-sensitized solar cells (DSSCs) by Miyasaka and co-workers.[8] In the following years, solid-state perovskite-based solar cells have risen to the forefront of thin film photovoltaics research, recently reaching certified efficiencies of 20.1%.[2] Despite the intense research in the field of photovoltaics, the potential use of $MAPbI_3$ in photodetectors is still largely unexplored.[3,4] This is partly due to the relatively high intrinsic resistivity and thus low photoelectron collection efficiency of $MAPbI_3$.[9] This shortcoming of $MAPbI_3$ was overcome by Hu et al.[3] by depositing a pure film of $MAPbI_3$ nanoparticles on a flexible indium tin oxide coated polyethylene terephthalate (ITO/PET) substrate. Accordingly responsivities as high as ≈3.5 A W^{-1} have been attained. An additional 50-fold improvement has been shown by replacing ITO/PET substrate by graphene in hybrid $MAPbI_3$/graphene photodetectors by Lee and co-workers.[4] This increase is partially attributed to the superior electronic characteristics of graphene over ITO/PET, but more importantly to a photodoping/gating effect.[4,10]

The electronic performance of graphene, however, is known for its sensitivity to chemical alterations. In particular, the carrier mobility in graphene changes by orders of magnitude due to the random surface potentials imposed by the substrate and the coating layer. In order to unravel the true photodetection potential of $MAPbI_3$/graphene heterostructures, a precise control of the $MAPbI_3$–graphene contacts is required. To this end, we have microengineered devices where a network of $MAPbI_3$ nanowires ($MAPbI_3NW$) has been combined with CVD-grown monolayer graphene. These phototransistors showed responsivities as high as 2.6×10^6 A W^{-1}, i.e., a value four orders of magnitude higher than existing literature reports.

An $MAPbI_3$ nanowire/graphene phototransistor was constructed from a network of perovskite nanowires deposited by the slip-coating method reported by Horváth et al.[9] onto a single-layer graphene field-effect transistor (FET). (Detailed description of the graphene–FET fabrication is given in Figure S2, Supporting Information) A combined optical and scanning electron microscope (SEM) micrograph of a representative device is shown in **Figure 1**a. Raman analysis of the graphene layer shows a threefold increase of the D-peak (I_D) over G-peak (I_G) ratio before and after covering the graphene with a network of perovskite nanowires (Figure 1b). This may imply the formation of C—I bonds on the as-grown graphene.[11] These additional scattering centers significantly modify the transfer characteristics of the devices (Figure 1c). The pristine graphene FET showed p-doped behavior with a charge neutrality point (Dirac point) above 50 V. This is attributed to the reactions of defects and poly(methyl methacrylate (PMMA) residues with p-doping chemical vapor adsorbents such as H_2O and CO.[12] The pristine graphene did not show measurable photoresponse at 633 nm illumination (details in Figure S3, Supporting Information). As depicted in Figure 1d, the Dirac point of the single-layer graphene transistor shifted heavily towards more

M. Spina, M. Lehmann, Dr. B. Náfrádi, Dr. L. Bernard, E. Bonvin, Dr. R. Gaál, Prof. L. Forró, Dr. E. Horváth
Laboratory of Physics of Complex Matter (LPMC)
Ecole Polytechnique Fédérale de Lausanne
1015 Lausanne, Switzerland
E-mail: endre.horvath@epfl.ch

Dr. A. Magrez
Crystal Growth Facility
Ecole Polytechnique Fédérale de Lausanne
1015 Lausanne, Switzerland

DOI: 10.1002/smll.201501257

www.MaterialsViews.com

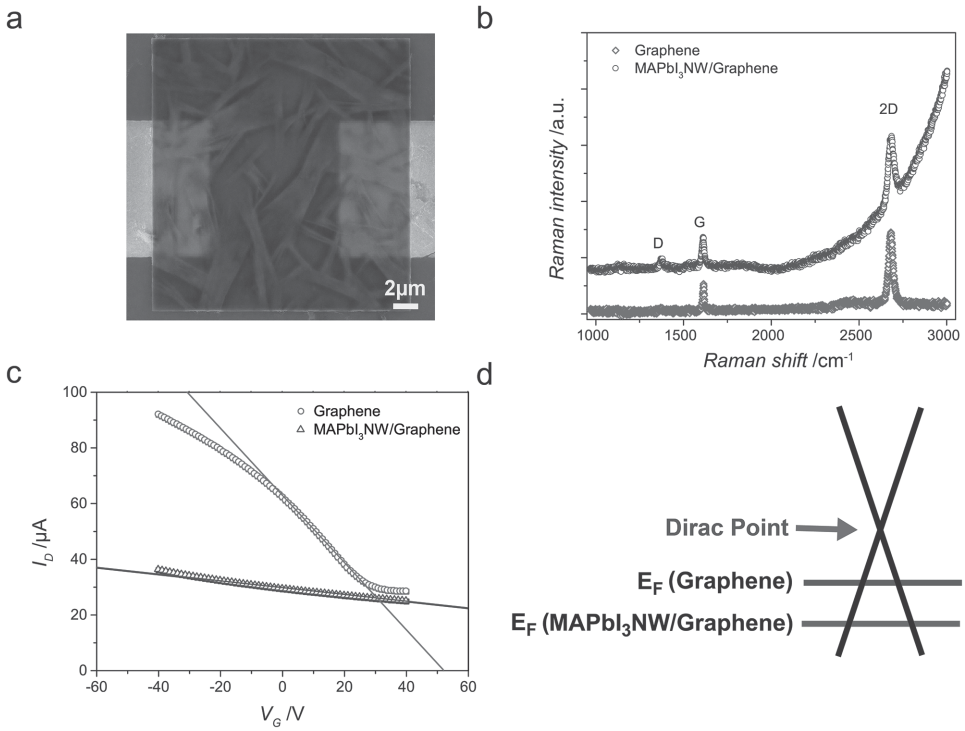

Figure 1. a) Combined optical and SEM image of a representative device showing a random percolating network of $MAPbI_3$NWs. b) Raman spectra of the graphene before (paler line) and after (darker line) the deposition of the $MAPbI_3$ nanowires (spectra are vertically shifted for clarity). c) Transfer characteristic of a representative device without illumination, before (paler line) and after (darker line) the deposition of the network of $MAPbI_3$ nanowires. d) Dirac cone scheme of the graphene before (paler line) and after (darker line) the hybridization. Note, that the pristine graphene FETs did not show measurable photocurrent under the illumination with 633 nm and 42.5 nW mm^{-2}.

positive voltages after the slip-coating of $MAPbI_3$ nanowires from DMF solution indicating a significant chemical doping of graphene by $MAPbI_3$. Additionally, the charge carrier mobility of graphene was lowered by a factor of 10 as a consequence of $MAPbI_3$NW deposition indicating the appearance of a significant random potential at atomic length scales on the $MAPbI_3$NW/graphene interface. As we will show, both of these two decrease the responsivity.

The device photoelectrical response was tested under broadband illumination conditions using a halogen lamp coupled with a monochromator with intensities at 633 nm from 3.3 pW (0.65 nW mm^{-2}) to 212.5 pW (42.5 nW mm^{-2}) (schematic representation shown in **Figure 2**a). Under light illumination, electron-hole pairs were generated in the $MAPbI_3$ nanowires and separated by the internal electric field due to the work function mismatch between graphene and the perovskite nanowire network; analogous to what was reported by Konstantatos et al. for the graphene/PbS junction.[13] Positive charge carriers were injected into the graphene while the negative charges accumulated in the nanowires acted as an additional light tunable gate that further decreased the Fermi energy of graphene.[3,14] (Figure 2b).

Wavelength-dependent photocurrent measurements (spectral sensitivity) revealed a central role of $MAPbI_3$NWs in the photon-induced carrier generation (Figure 2c and Figure S6, Supporting Information). The photocurrent generation is observed in the wavelength range characteristic for the band structure (onset ≈770 nm, ≈1.6 eV) of $MAPbI_3$. The number of photoinduced charge carriers increases proportionally with the applied drain voltage without any sign of saturation, at all measured incident light intensities (Figure 2d). We estimate the responsivity of the hybrid device to be as high as 2.6×10^6 A W^{-1} at V_D = 10 mV and 3 pW. According to the authors' knowledge, at present, this champion device has the highest responsivity values among perovskite-based photodetectors. Considerably, the observed value is seven orders of magnitude higher than that of the commercially available Si detectors (0.6 A W^{-1}) and four orders of magnitude higher than the responsivity of hybrid graphene/$MAPbI_3$ nanoparticles photodetector reported very recently.[4] We attribute this enormously enhanced responsivity to engineering the contact between the $MAPbI_3$NW sensitizer and the graphene electrode by synthetizing a $MAPbI_3$ nanowire network.

Now we turn to the discussion of the limiting factors of the responsivity and comment on further possibilities to improve the responsivity of $MAPbI_3$ nanowire/graphene photodetectors. It is widely accepted that the charge collection efficiency is one of the most critical parameters in photodetectors.[15] Overall, the recombination losses can be often directly correlated to the transit time, hence the channel length of the device and the electric field used to extract the photogenerated charges from the device. Here, we tested the photoelectrical response of about 20 devices with different channel lengths (ranging from 10 to 120 μm) under a 633 nm red laser illumination of 2.5 W cm^{-2}. For a fixed source-to-drain electric field of 8 V cm^{-1}, the photoresponse of the devices was about 10 times higher when their dimensions were five times

DOI: 10.1002/smll.201501257

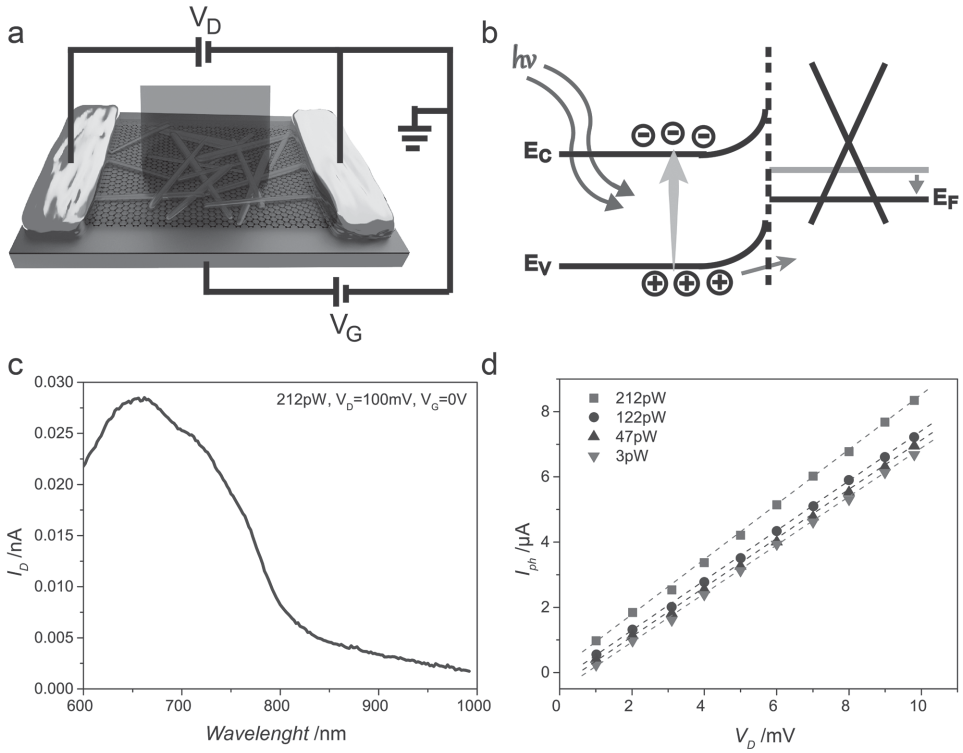

Figure 2. a) Schematic representation of the measurement setup. b) Electronic band diagram of the MAPbI3NW/graphene heterojunction for gate voltages (V_G) lower than the charge neutrality point. E_V and E_C indicate the valence and conduction band of $MAPbI_3$NW, respectively. The injection of the photogenerated holes into the graphene is facilitated by the built-in field formed at the junction. The electrons accumulated in the perovskite nanowires generate an electric field that shifts further Fermi level (E_F) of graphene. c) Variation of the current in the device as a function of the wavelength (spectral sensitivity) of the incident light (note, that the data are qualitative only). The sharp increase below ≈770 nm, i.e., below the bandgap of $MAPbI_3$NW testifies that the photosensitivity is due to the $MAPbI_3$NW network. d) Output characteristic of the photodetector for different incident light intensities. The linear behavior and absence of saturation indicate the possibility that higher responsivity can be reached increasing the voltage between the two metal contacts.

smaller (**Figure 3**a). We attribute this 10-fold increase in responsivity to a more effective collection of the photogenerated charge carriers in the device. The scaling law indicates the crucial role of $MAPbI_3$ nanowire/graphene interface quality and demonstrates that miniaturization is a way forward to further improve the photodetector performance.

The undeniable role of the quality of $MAPbI_3$NW/graphene interface is also indicated by the time dependence of the photocurrent. The time response showed characteristic rise and fall times of ≈55 s and ≈75 s of the photocurrent, respectively (Figure 3b). Even though our perovskite nanowire-based hybrid photodetector is faster than other highly efficient graphene-based photodetectors,[10] the measured response time values are still much longer than the instrinsic photoresponse time of the methylammonium lead iodide perovskite.[16] and other perovskite-based photodetectors (see details in the Supporting Information: Comparative table of the performances of the best-in-class graphene and $MAPbI_3$ photodetectors).[3,4,9] As may be observed in Figure 3b the response times can be divided into two components. The fast component has characteristic time scales of ≈5 s (corresponding to ≈70% decay) and the slow component attributed to the multiplicity of charge traps in the nanowire film stems from different surface states.[17] It is reasonable to suppose that the improvement of the interface between the graphene and the nanowires and the reduction of the defect density states could significantly increase the responsivity, decrease the trapped electron lifetime, hence, reduce the characterestic response times from tens of seconds down to a few milliseconds or shorter.

Currently little is known about the physicochemical properties of the interfaces of organolead halide perovskites and carbon nanostructures such as fullerenes, graphene, and carbon nanotubes. In solid-state perovskite-based solar cells, integrated carbon nanomaterials of different dimensionalities play a beneficial role on the photovoltaic device stability (i.e., reduced *I–V* hysteresis, anticorrosive effect, efficient charge collector, and moisture protection), as recently demonstrated by several research groups.[18] Nevertheless, little is known about the physicochemical properties of these interfaces and their role in the charge-transfer process. In order to test the $MAPbI_3$NW/graphene electronic junction, we have fabricated two terminal longitudinal devices with perovskite nanowire active layer and two graphene contacts (Figure S3, Supporting Information). These devices showed linear *I–V* characteristics proving that there is a non-rectifying ohmic-type contact between the CVD graphene and the $MAPbI_3$NW (Figure S4, Supporting Information). This result is somewhat surprising, since it is well known that, e.g., in circuit fabrication generating low-resistance ohmic contact allowing

DOI: 10.1002/smll.201501257

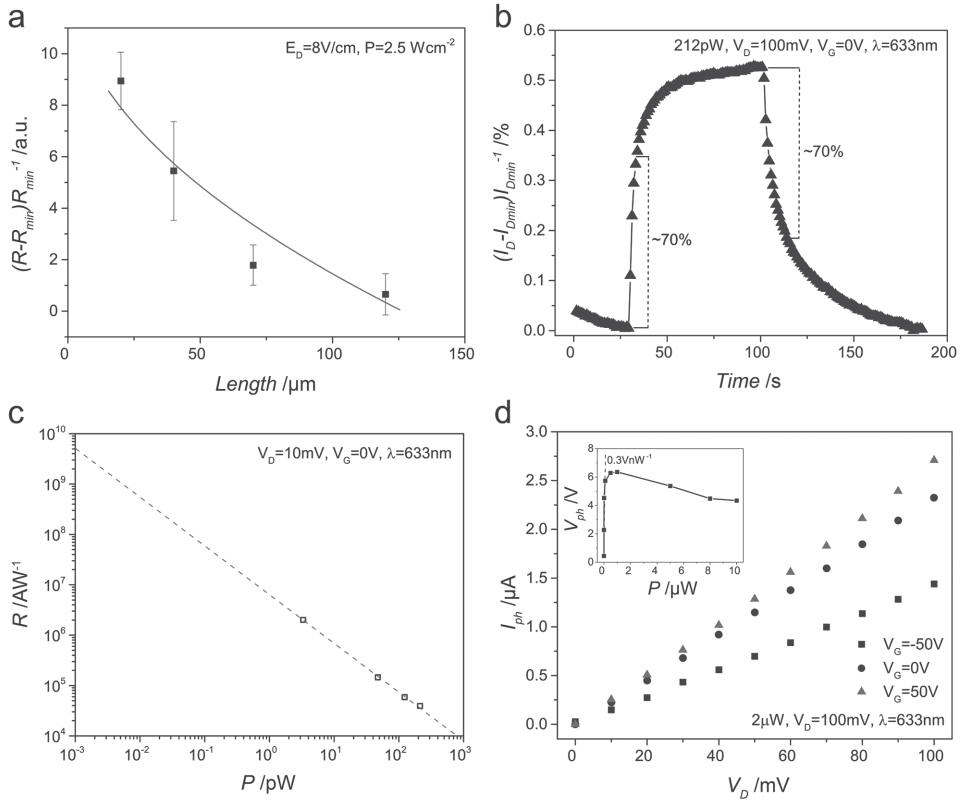

Figure 3. a) Relative variation of the responsivity as a function of the device length for a fixed source-to-drain electric field E = 0.83 V cm^{-1}. b) Time response of a representative device. Two regimes can be identified: a fast one corresponding to ≈70% decay (≈5 s) and a slow one of ≈75 s associated with the charge traps in nanowire film. c) Responsivity of the device for different incident light intensities. Dashed line shows extrapolation towards lower intensities. d) Photocurrent of the bottom-gated device as a function of both the applied bias and gate voltage. The performance of the device increases with both voltages. Inset presents the photogating V_{ph} as a function of light intensity. V_{ph} rises rapidly with increasing light intensity and saturates about 1 μW.

the photogenerated charges to flow easily in both directions between a metal and a semiconductor usually requires careful techniques. The strong reducing/oxidizing power of the highly concentrated ionic solution of methylammonium lead iodide in organic solvents brought in contact with graphene during the slip-coating process has twofold role in the ohmic contact formation. First, it acts as the source of perovskite crystallization. Second, during the nanowire growth, it creates a highly reducing environment (similar to high vacuum cleaning and thermal annealing) and acts as a local "etchant" by removing, dissolving the adsorbed impurities. The perovskite nanowires then start to grow on the graphene surface by classical supersaturation-induced nucleation and crystal growth. Importantly, the anisotropic crystal growth is guided by the organic solvent itself through and intermediate solvatomorph formation and subsequent solvent evaporation induced perovskite crystallization, ultimately resulting in the formation of low-resistance ohmic contacts between the two materials. Currently we are investigating the redox properties of methylammonium lead iodide solutions more in detail. Conclusive data will be reported later.

As it is depicted in Figure 3d, in the $MAPbI_3$NW/graphene transistor, the application of a transverse electric field (induced by the back-gate voltage V_G) modulates the photoresponsivity by tuning the graphene conducting channel. Application of V_G = 50 V increased the responsivity by 15% while inverting the voltage reduces the responsivity by about the same amount, indicating that reducing the shift of the graphene neutrality point enhances the responsivity. Future efforts, optimization and device engineering could result in more robust back-gate dielectrics sustaining larger electric fields. Overall, positive effect of augmented V_G on the response time is also expected.[13]

The photogating effect, i.e., the shift in the charge neutrality point of the graphene upon light illumination to the $MAPbI_3$NW/graphene interface is shown in Figure 3d inset. We estimated this shift by relating the photoinduced current variation to the values that the back-gate voltage should have to induce the same variation. As a consequence of the generated photocurrent, the shift of the Dirac point increases extremely fast for low intensities (Figure 3d inset). This is in good agreement with the observed reduction of the responsivity at high light-intensities, i.e., when the photogating effect is high.

The photocurrent shows no saturation as a function of the drain voltage (Figure 2d) suggesting that higher responsivities could be readily achieved by applying a larger longitudinal electric field.[19] Our hybrid device acts as a solid-state photomultiplier converting 1 incoming photon (at 633 nm) to ≈4 × 10^6 outgoing electrons. This suggests the potential

DOI: 10.1002/smll.201501257

application of this device as a room temperature single-photon detector as 1 photon s^{-1} illumination would generate 0.6 pA currents what is within the detection limit of commercial high-sensitivity current meters. Furthermore, these values were obtained at very low-longitudinal electric fields ($\approx$10 V cm^{-1}) meaning that single-electron detection could be achieved even with low-power consumption.

Finally the photoresponse of the detector dramatically increases at very low light intensities. The maximum responsivity of $\approx 2.6 \times 10^6$ A W^{-1} was measured with an incident power of 3.3 pW (Figure 3c). Assuming the observed relation between the photocurrent and the incident power (Figure 3c) is valid even at lower power intensities, i.e., in the fW range, efficiencies of the order of 10^{10} A W^{-1} could be achieved at room temperature.

In conclusion, we fabricated the first hybrid $MAPbI_3$ nanowire/graphene photodetector. The measured device photoresponsivity was as high as 2.6×10^6 A W^{-1} that is four orders of magnitude higher than the best hybrid perovskite photodetector reported by Lee et al.[4] and comparable to the best hybrid graphene photodetectors reported so far.[10,13] under similar operating conditions. We attribute these very high device performances mainly to the nanowire perovskite morphology. The drastic enhancement of the responsivity at very low light intensities (pW) suggests the use of $MAPbI_3$ nanowire/graphene devices as low-light imaging sensors and single-photon detectors.

Experimental Section

Photoelectric Characterization: The photoelectric response measurements of the fabricated hybrid devices were performed using a standard DC technique. The light sources used were a red laser beam (λ = 633 nm) with a spot size of about 4 mm and a halogen lamp connected to a monochromator for the characterization under broadband illumination conditions. All the measurements were performed at room temperature in ambient conditions.

Spectral Responsivity Measurement: Photocurrent as a function of incident light energy was measured in a two-terminal geometry with fixed bias voltage. For photocurrent spectra, a low-intensity monochromatic light was selected by a MicroHR grid monochromator from a halogen lamp. The wavelength resolution (FWFM) of the 600 g mm^{-1} grating was 10 nm.

Supporting Information

Supporting Information is available from the Wiley Online Library or from the author.

Acknowledgements

This work was founded by the Swiss National Science Foundation. Device fabrication was carried out in part in the EPFL Center for Micro/Nanotechnology (CMI).

[1] M. Liu, M. B. Johnston, H. J. Snaith, *Nature* **2013**, *501*, 395.
[2] G. Niu, X. Guo, L. Wang, *J. Mater. Chem. A* **2015**, DOI: 10.1039/C5TA02779A.
[3] X. Hu, X. Zhang, L. Liang, J. Bao, S. Li, W. Yang, Y. Xie, *Adv. Funct. Mater.* **2014**, *24*, 7373.
[4] Y. Lee, J. Kwon, E. Hwang, C.-H. Ra, W. J. Yoo, J.-H. Ahn, J. H. Park, J. H. Cho, *Adv. Mater.* **2015**, *27*, 41.
[5] J.-Y. Jeng, Y.-F. Chiang, M.-H. Lee, S.-R. Peng, T.-F. Guo, P. Chen, T.-C. Wen, *Adv. Mater.* **2013**, *25*, 3727.
[6] M. M. Lee, J. Teuscher, T. Miyasaka, T. N. Murakami, H. J. Snaith, *Science* **2012**, *338*, 643.
[7] a) S. D. Stranks, G. E. Eperon, G. Grancini, C. Menelaou, M. J. P. Alcocer, T. Leijtens, L. M. Herz, A. Petrozza, H. J. Snaith, *Science* **2013**, *342*, 341; b) G. Xing, N. Mathews, S. Sun, S. S. Lim, Y. M. Lam, M. Grätzel, S. Mhaisalkar, T. C. Sum, *Science* **2013**, *342*, 344.
[8] A. Kojima, K. Teshima, Y. Shirai, T. Miyasaka, *J. Am. Chem. Soc.* **2009**, *131*, 6050.
[9] E. Horváth, M. Spina, Z. Szekrényes, K. Kamarás, R. Gaal, D. Gachet, L. Forró, *Nano Lett.* **2014**, *14*, 6761.
[10] K. Roy, M. Padmanabhan, S. Goswami, T. P. Sai, G. Ramalingam, S. Raghavan, A. Ghosh, *Nat. Nano* **2013**, *8*, 826.
[11] Z. Yao, H. Nie, Z. Yang, X. Zhou, Z. Liu, S. Huang, *Chem. Commun.* **2012**, *48*, 1027.
[12] a) F. Schedin, A. K. Geim, S. V. Morozov, E. W. Hill, P. Blake, M. I. Katsnelson, K. S. Novoselov, *Nat. Mater.* **2007**, *6*, 652; b) Y. Dan, Y. Lu, N. J. Kybert, Z. Luo, A. T. C. Johnson, *Nano Lett.* **2009**, *9*, 1472.
[13] G. Konstantatos, M. Badioli, L. Gaudreau, J. Osmond, M. Bernechea, F. P. G. de Arquer, F. Gatti, F. H. L. Koppens, *Nat. Nano* **2012**, *7*, 363.
[14] Y. Q. Huang, R. J. Zhu, N. Kang, J. Du, H. Q. Xu, *Appl. Phys. Lett.* **2013**, DOI: 10.1063/1.4824113.
[15] M. Bass, *Handbook of Optics: Fundamentals, Techniques, and Design*, Vol. *1*, McGraw-Hill, New York 1994.
[16] A. Marchioro, J. Teuscher, D. Friedrich, M. Kunst, R. van de Krol, T. Moehl, M. Gratzel, J.-E. Moser, *Nat. Photonics* **2014**, *8*, 250.
[17] G. Konstantatos, L. Levina, A. Fischer, E. H. Sargent, *Nano Lett.* **2008**, *8*, 1446.
[18] a) Y. Shao, Z. Xiao, C. Bi, Y. Yuan, J. Huang, *Nat. Commun.* **2014**, *5*, 1; b) A. Abrusci, S. D. Stranks, P. Docampo, H.-L. Yip, A. K. Y. Jen, H. J. Snaith, *Nano Lett.* **2013**, *13*, 3124; c) Z. Li, S. A. Kulkarni, P. P. Boix, E. Shi, A. Cao, K. Fu, S. K. Batabyal, J. Zhang, Q. Xiong, L. H. Wong, N. Mathews, S. G. Mhaisalkar, *ACS Nano* **2014**, *8*, 6797; d) S. N. Habisreutinger, T. Leijtens, G. E. Eperon, S. D. Stranks, R. J. Nicholas, H. J. Snaith, *Nano Lett.* **2014**, *14*, 5561; e) J. T.-W. Wang, J. M. Ball, E. M. Barea, A. Abate, J. A. Alexander-Webber, J. Huang, M. Saliba, I. Mora-Sero, J. Bisquert, H. J. Snaith, R. J. Nicholas, *Nano Lett.* **2014**, *14*, 724.
[19] C.-H. Liu, Y.-C. Chang, T. B. Norris, Z. Zhong, *Nat. Nano* **2014**, *9*, 273.

Received: May 4, 2015
Revised: June 12, 2015
Published online: